

Mathematical Modelling and Description of the Technological Process of Aluminum Anodic Oxidation by Using the Neural Networks

A. Vagaská, P. Michal, I. Bukovský, M. Gombár and J. Kmec

Abstract—In this paper the usage of neural networks and Design of Experiments methodology in order to control and optimize the technological process of aluminium anodic oxidation is presented. The influence of the input factors on the resulting AAO (anodic aluminum oxide) film thickness was monitored at defined current density of $4.00 \text{ A}\cdot\text{dm}^{-2}$, $5.00 \text{ A}\cdot\text{dm}^{-2}$ and $6.00 \text{ A}\cdot\text{dm}^{-2}$. The thickness of the formed AAO layer has been investigated as the relationship of physical and chemical factors acting during the anodic oxide process. A higher-order neural unit based on the iterative Levenber-Maquardt algorithm was used to evaluate experimentally obtained data in order to predict the thickness of the resulting AAO layer and determine the optimum selection of process conditions.

Keywords—neural network, artificial intelligence, surface treatment, anodizing

I. INTRODUCTION

PURE aluminum and its alloys, such as weight-saving materials, play an increasingly important role of technical, technological and economic terms [1] in the aerospace and automotive industries [2], where lightweight and rigid structure are preferred [3]. The usage of these materials for moving parts is limited due to their low abrasion and wear resistance. To improve tribological properties of such materials, the surface of these components is treated by anodic oxidation process, which also improves the corrosion resistance [1], [2]. The thickness of the AAO film formed on the aluminum substrates is one of the main indicators of corrosion protection and overall durability of so prefinished profiles. For these reasons the anodic oxidation of aluminum has received great attention of considerable amount of researchers. For example, the formation of AAO layers was studied in [4], growth rate of the oxide was studied in [5] and

Alena Vagaská, Technical University of Kosice, Faculty of Manufacturing technologies with seat in Presov, Department of Mathematics, Informatics and Cybernetics, Presov, Slovak Republic, (alena.vagaska@tuke.sk)

Peter Michal, Technical University of Kosice, Faculty of Manufacturing technologies with seat in Presov, Department of Mathematics, Informatics and Cybernetics, Presov, Slovak Republic, (peter.michal@tuke.sk)

Ivo Bukovský, Czech Technical University in Prague, Faculty of Mechanical Engineering, Department of Instrumentation and Control Engineering, Prague, Czech Republic, (ivo.bukovsky@fs.cvut.cz)

Miroslav Gombár, University of Presov in Presov, Faculty of Management, Department of Management, Presov, Slovak Republic, (gombar.mirek@gmail.com)

Ján Kmec, University of Presov in Presov, Faculty of Management, Department of Management, Presov, Slovak Republic, (jan.kmec@unipo.sk)

structure of the formed AAO layer was investigated in [6]. The basic tool that allows us to observe the effect of input variables (factors) on output variable (response) is Design of Experiments [7, 8, 9, 10]. The optimum selection of process conditions is an extremely important issue as the determine surface quality of the manufactured parts [11, 12, 13, 14]. The mathematical modeling of the process involves several parameters that may lead to difficult analytical solution [15, 16, 17, 18, 19]. On the other hand, the use of artificial intelligence (neural networks theory) for evaluating the experiment results is justified mainly due to higher speed and accuracy of behavior prediction of observed process compared to conventional statistical evaluation methods [20, 21, 22, 23, 24].

II. EXPERIMENTAL

A. Preparation of samples

Alloy EN AW 1050 - H24 with dimensions $101 \times 70 \times 1 \text{ mm}$ was used for the specimens. Each applied specimen was degreased in a 38.00% solution of NaOH at 55.00 to $60.00 \text{ }^\circ\text{C}$ for 2 minutes and stained in a 40.00% solution of NaOH at the temperature 45.00 - $50.00 \text{ }^\circ\text{C}$ for 0.50 min. Consequently, the specimen was immersed in a nitric acid bath (4.00% HNO_3) at the temperature 18.00 to $24.00 \text{ }^\circ\text{C}$ for 1.00 minute. Between each operation, the sample was rinsed with distilled water.

B. Anodizing conditions

The electrolyte solution containing sulphuric acid p.a., oxalic acid p.a. and alumina oxide p.a. was used for anodic oxide process. Individual concentrations were based on the Design of Experiments (DoE) methodology corresponding to the central composite design for six factors, which determined operating conditions of anodizing process (the electrolyte temperature, the size of an applied voltage and duration of oxidation). Tab. 1 presents the conversion of factor levels between coded scale and natural one. Such areas of the sample surface where the current density was $4 \text{ A}\cdot\text{dm}^{-2}$, $5 \text{ A}\cdot\text{dm}^{-2}$ or $6 \text{ A}\cdot\text{dm}^{-2}$ were indicated after the anodizing process was finished. Furthermore, 9 points were indicated at a distance of 5mm, 10mm, 15mm, 20mm, 25mm, 30mm, 35mm, 40mm and 45 mm from the bottom edge of each sample. The thickness of the formed anodic oxide films was measured in these points.

Table 1 conversion of factors levels between coded scale and natural one

Factors denotation	Factor level				
	-2.37	-1	0	+1	+2.37
$x_1-H_2SO_4$ [mol·l ⁻¹]	0.34	1.33	2.04	2.75	3.74
$x_2-C_2H_2O_4$ [mol·l ⁻¹]	0.01	0.07	0.12	0.16	0.23
x_3-Al^{3+} [mol·l ⁻¹]	0.01	0.19	0.32	0.46	0.62
x_4-T [°C]	-1.78	12.00	22.00	32.00	45.78
x_5-t [min]	6.22	20.00	30.00	40.00	53.77
x_6-U [V]	5.24	8.00	10.00	12.00	14.76

A higher-order neural unit (HONU), especially the 3rd order HONU [26] based on the iterative Levenberg-Marquardt (LM) algorithm [27] was used to determine the influence of input factors on the thickness of the final AAO layer. This algorithm is often used for training technique of the neural unit. It is a process of updating individual weights \mathbf{w} in a predetermined number of steps to achieve a minimum difference between the actual and calculated values of observed variable [28]. This process is described by (1) – (8). The vector \mathbf{u} of neural inputs is created by taking the partial derivatives of each output in respect to each weight (1) – (3). The equation describing the investigated model is the characteristic equation of given type of neural unit (1st order HONU, 2nd order HONU a 3rd order HONU) for observed factors $x_1, x_2, x_3, x_4, x_5, x_6$. The Levenberg-Marquardt algorithm consists in solving (4), where the Jacobian \mathbf{J} is the matrix of dimension $n \times m$ (5), where n is the length of the input vector \mathbf{u} of the neural unit (n is the number of neural inputs) and m is the total number of parameters intended for the learning procedure. The vector of neural inputs as well as the Jacobian is defined in the first step of the learning procedure and they remain constant in all subsequent steps of learning. In (4) there is the weight update vector $\Delta\mathbf{w}$ that we want to find, \mathbf{e} is the error vector containing the output errors for each input vector used on training the network, $1/\mu$ is the Levenberg's damping factor which tell us by how much we should change our network weights to achieve a (possibly) better solution. The $\mathbf{J}^T \cdot \mathbf{J}$ matrix can also be known as the approximated Hessian, the \mathbf{I} is an identity matrix of diagonal length equal to the number of neural weights (matrix of dimension $n \times n$), μ is the learning rate.

The vector \mathbf{y}' of neural outputs is defined as the dot product of vectors \mathbf{w} and \mathbf{u} (6), the size of the individual weight is set in the first step randomly. After calculating the output vector is calculated error vector \mathbf{e} as the difference between the actual value of the observed variable and the calculated one by the neural units (6). Then the weight update vector $\Delta\mathbf{w}$ is determined by (4). The size of the learning rate μ depends on how quickly and how accurately the neural unit is able to learn. At higher values of learning rate the neural unit will

learn faster but there is a risk of instability respectively a risk of model oscillation. At lower values of learning rate the calculation is more accurate but the learning process requires a larger number of iterations [16]. After calculating the weight-updates, the adaptation of the weights of input factors occurs. This is the end of first step (respectively the first iteration) of the learning process of neural unit using iterative Levenberg-Marquardt (LM) algorithm optimization. The learning process of neural units continues by calculating the vector of neural outputs \mathbf{y} using the new (adapted) weights.

$$u_i = \frac{\partial y_{HONU}}{\partial w_i} \quad (1)$$

$$\mathbf{u} = \begin{bmatrix} u_1 \\ u_2 \\ \vdots \\ u_n \end{bmatrix} \quad (2)$$

$$\mathbf{w} = \begin{bmatrix} w_1 \\ w_2 \\ \vdots \\ w_n \end{bmatrix} \quad (3)$$

$$\Delta\mathbf{w} = \left(\mathbf{J}^T \cdot \mathbf{J} + \frac{1}{\mu} \cdot \mathbf{I} \right)^{-1} \cdot \mathbf{J}^T \cdot \mathbf{e} \quad (4)$$

$$\mathbf{J} = \begin{bmatrix} \mathbf{u}^T_1 \\ \mathbf{u}^T_2 \\ \vdots \\ \mathbf{u}^T_m \end{bmatrix} = \begin{bmatrix} u_{1,1} & u_{2,1} & \cdots & u_{n,1} \\ u_{1,2} & u_{2,2} & \cdots & u_{n,2} \\ \vdots & \vdots & \ddots & \vdots \\ u_{1,m} & u_{2,m} & \cdots & u_{n,m} \end{bmatrix} \quad (5)$$

$$\mathbf{y}' = \mathbf{w} \cdot \mathbf{u} \quad (6)$$

$$\mathbf{e} = \mathbf{y} - \mathbf{y}' \quad (7)$$

$$\mathbf{w} = \mathbf{w} + \Delta\mathbf{w} \quad (8)$$

After the learning process of neuron unit is done, we get a computational model that describes the thickness of AAO layer with equation 9 and equation 10 for linear neural unit, equation 11 and equation 12 for quadratic neural unit and equation 13 and equation 14 for cubic neural unit.

$$th_{LNUth} = \frac{3}{1 + e^{-\alpha_{LNU}}} 3 \cdot std_y \quad (9)$$

$$\alpha_{LNU} = \sum_{i=1}^n (u_{iLNU} \cdot w_{iLNU}) \quad (10)$$

$$th_{QNU} = \frac{3}{1 + e^{-\alpha_{QNU}}} 3 \cdot std_y \quad (11)$$

$$\alpha_{QNU} = \sum_{i=1}^n (u_{iQNU} \cdot w_{iQNU}) \quad (12)$$

$$th_{CNU} = \frac{3}{1 + e^{-\alpha_{CNU}}} 3 \cdot std_y \quad (13)$$

$$\alpha_{CNU} = \sum_{i=1}^n (u_{iCNU} \cdot w_{iCNU}) \quad (14)$$

Where th is final thickness of oxide layer, α is preliminary thickness of oxide layer, u_i is a combination of input factors levels (in coded scale), w_i are weights for combinations of input factors and std_y is standard deviation of real values (measured layer thickness vector y) divided by 3. Calculated thickness of oxide layer is expressed in $mm \cdot 10^{-3}$.

III. RESULTS AND DISCUSSION

Setting of simulation was used as follows. Letter y means a mean value of the layer thickness measured in points at a distance of 10.00 mm, 20.00 mm, 30.00 mm and 40.00 mm from bottom margin of each testing sample. Current density was set at 4.00, 5.00 and $6.00 \text{ A} \cdot \text{dm}^{-2}$. For learning process were used 36 values of randomly measured thickness for one setting of the current density. Ten remaining values of the thickness were used during model validation process. That value ratio was chosen experimentally, according to goal to find the lowest possible number of training values sufficient enough to provide the prediction model with adequate precision. With the greater amount of training data we were not able to clearly validate the model. During evaluation of the experiment results, it was possible to mathematically describe an influence of the input factors on the resulted thickness of the AAO layer via neural unit. The unit used cubic model with small number of data. According to the theory of the neural networks the third order HONU is able to surely describe highly nonlinear model only via large amount of training data. Respectively, with smaller amount of training data is necessary to choose a neural unit with lower order. When we tried to use lower order neural unit (linear model, quadratic model) a big error of prediction model occurred. The error occurred during the training process and became even greater during validation process. In Tab. 2 it is possible to see how much is the model able to describe the influence of state values, which were not in training data. In the table are statistical stats of correctness of cubic, quadratic and linear model. The table 2 also contains suitability (or correctness) of usage the particular evaluation models for estimating of the AAO layer thickness. The sum of square errors of 3rd Order HONU was 7.50 times lower than the sum of square errors of 2nd Order HONU at the current

density of $4.00 \text{ A} \cdot \text{dm}^{-2}$. At the current density of $5.00 \text{ A} \cdot \text{dm}^{-2}$ the sum of square errors was even 8.33 times lower, and 7.40 times lower at the current density of $6.00 \text{ A} \cdot \text{dm}^{-2}$. Usage of 3rd Order HONU is 5.93 times more accurate than 1st Order HONU at the current density of $4.00 \text{ A} \cdot \text{dm}^{-2}$, 10.41 times more accurate if the current density was $5.00 \text{ A} \cdot \text{dm}^{-2}$ and 10.67 times more accurate at the current density of $6.00 \text{ A} \cdot \text{dm}^{-2}$. While 3rd Order HONU neural unit was used, correlation index of the input factors and the AAO result thickness reached levels 96.67 %, 97.56 % and 98.33 % at the current densities of $4.00 \text{ A} \cdot \text{dm}^{-2}$, $5.00 \text{ A} \cdot \text{dm}^{-2}$ and $6.00 \text{ A} \cdot \text{dm}^{-2}$. In comparison with 2nd Order HONU the correlation index is approximately 7.14% higher and about 12.64% in comparison with results of 1st Order HONU.

Table 2. Selected indicators of the accuracy of developed models

Model	Current density [$\text{A} \cdot \text{dm}^{-2}$]	SSE [-]	MSE [-]	R ² [%]	R [%]
Cubic 3 rd Order HONU	4.00	87.51	2.37	93.45	96.67
	5.00	62.42	1.69	95.17	97.56
	6.00	45.31	1.22	96.69	98.33
Quadratic 2 nd Order HONU	4.00	656.75	17.75	78.79	88.76
	5.00	519.70	14.05	81.03	90.02
	6.00	335.50	79.07	85.30	92.36
Linear 1 st Order HONU	4.00	518.69	14.02	68.31	82.65
	5.00	649.87	17.56	78.91	88.83
	6.00	496.92	13.43	69.16	83.16

Fig.1, Fig.2 and Fig .3 show the simulation error (a difference between measured and calculate value of the AAO layer thickness) of individual mathematical model (1st order HONU neural unit Fig.1, 2nd order HONU neural unit Fig.2, 3rd order HONU neural unit Fig.3) developed for the current density of $4.00 \text{ A} \cdot \text{dm}^{-2}$.

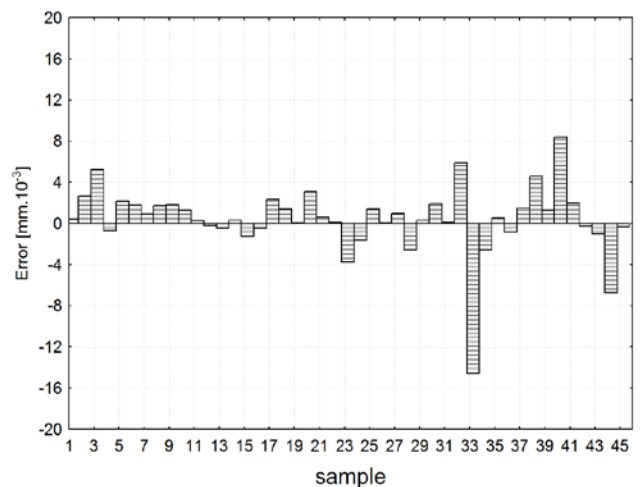


Fig. 1. Simulation error of 1st order HONU neural unit at observed current density of $4.00 \text{ A} \cdot \text{dm}^{-2}$

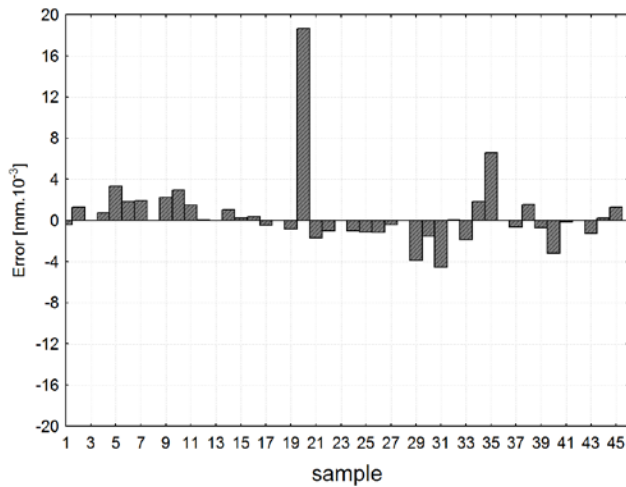


Fig. 2. Simulation error of 2nd order HONU neural unit at observed current density of 4.00 A·dm⁻²

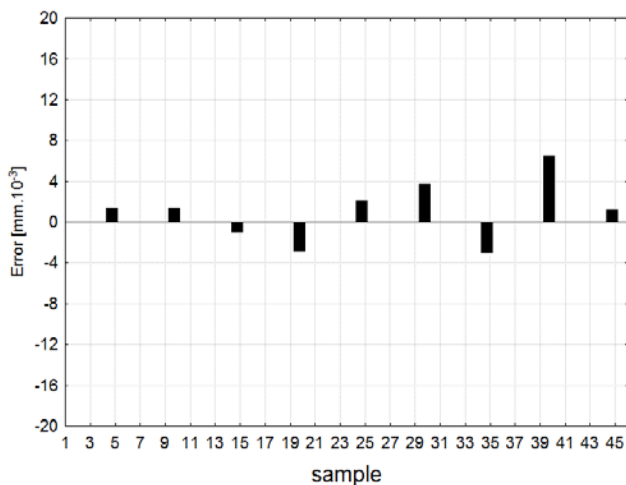


Fig. 3. Simulation error of 3rd order HONU neural unit at observed current density of 4.00 A·dm⁻²

As we can see in the figures, the biggest errors appear in the estimation of AAO layer thickness via 1st Order HONU, which describes the influence of input parameters using only linear function (Fig. 1). The 2nd Order HONU (Fig. 2) shows lower error of estimation the AAO layer thickness. This neural unit describes the impact on the response by using quadratic function. Usage of that kind of neural unit could be useful in industry to obtain approximate information about input factors influence on the result of technological process. Unfortunately, that neural unit shows the highest absolute calculation error in comparison with other tested neural units. Particularly in estimation of the AAO layer thickness of sample no. 20 the evaluated value is about $18.67 \text{ mm} \cdot 10^{-3}$ greater than the actual value of measured thickness of the AAO layer. That means a big chance for similarly high error during calculation with the input factors which were not included in the experiment. For that reason, the 2nd Order HONU neural unit is insufficient for real industry control. The best results are shown by using the 3rd order HONU neural unit (Fig.3), which describes the

influence of input factors on the AAO layer thickness by using cubic function. In other words, that neural unit is the most nonlinear from tested units and that cause its ability to estimated so complicated model with high precision.

Fig. 4, Fig. 5 and Fig. 6 describe the results of training process of neural units of 3rd order HONU of the obtained prediction model at current density 4.00 A·dm⁻² (Fig.4), 5.00 A·dm⁻² (Fig.5) and 6.00 A·dm⁻² (Fig.6). From these figures it is clearly seen how all points (values of the AAO layer thickness) used for training are laying on ideally straight line. That means, that the neural unit was able to learn how the input factors influence the resulting AAO layer thickness with almost absolute precision. The sum of square errors reached the value of $1.20 \cdot 10^{-11} \text{ mm}^2 \cdot 10^{-6}$ during training process at the current density of 4.00 A·dm⁻², the value of $1.60 \cdot 10^{-10} \text{ mm}^2 \cdot 10^{-6}$ at current density of 5.00 A·dm⁻² and value of $8.38 \cdot 10^{-9} \text{ mm}^2 \cdot 10^{-6}$ at current density of 6.00 A·dm⁻².

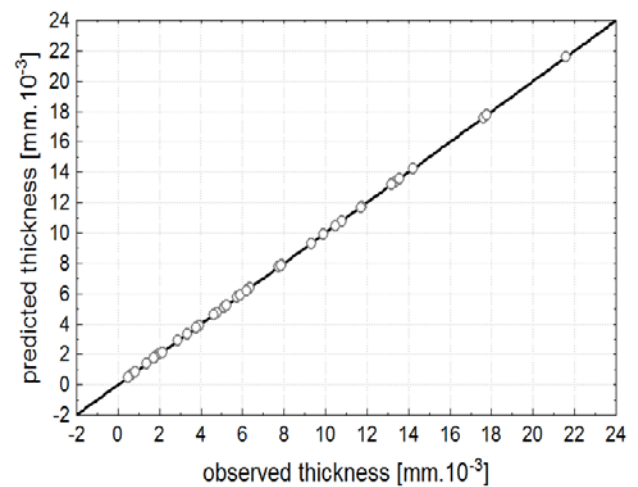


Fig. 4. Training process of 3rd order HONU at current density of 4.00 A·dm⁻²

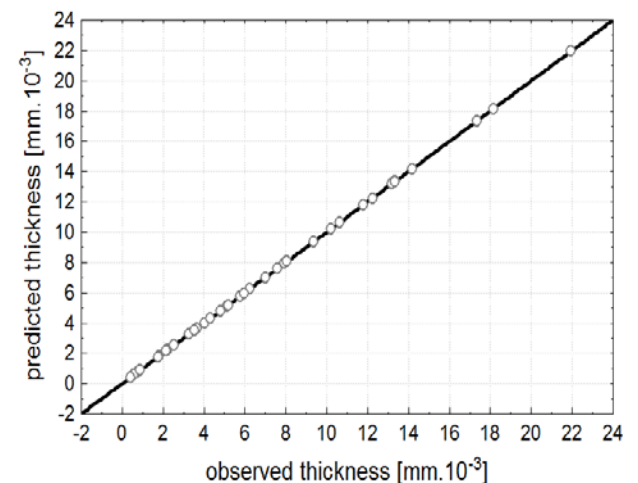


Fig. 5. Training process of 3rd order HONU at current density of 5.00 A·dm⁻²

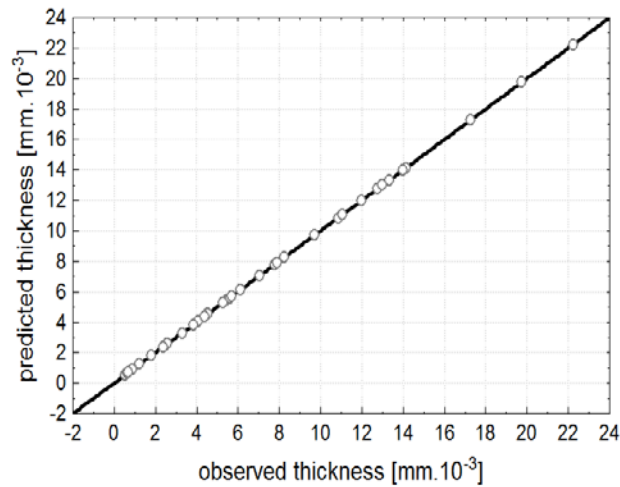


Fig. 6. Training process of 3rd order HONU at current density of 6.00 A·dm⁻²

Fig. 7, Fig. 8 and Fig. 9 describe the results of the verification process of the obtained prediction model at current density 4.00 A·dm⁻² (Fig.7), 5.00 A·dm⁻² (Fig.8) and 6.00 A·dm⁻²(Fig.9). During the validation process, it results in a difference between the measured value of AAO layer thickness and predicted value of AAO layer thickness, because the neural unit was not trained for that sort of combinations of the input factors. Those untrained values are close to error free straight line of prediction so we can conclude that the neural units are able to correct prediction of untrained inputs. It means that we do not need so much training data respectively specimens if we want describe influences of input factors to output of examined technological process of anodic oxidation of aluminum.

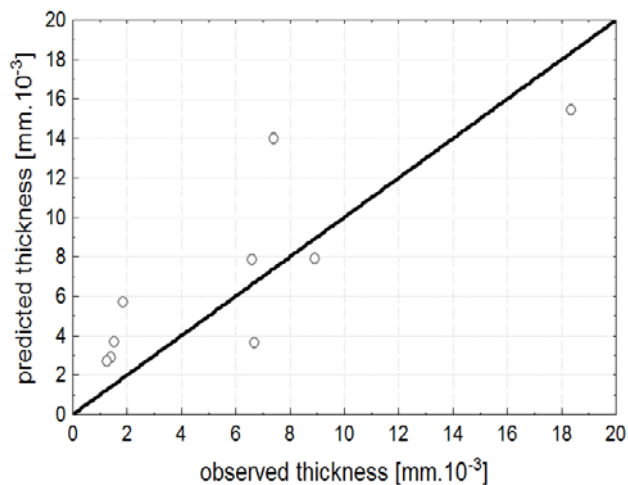


Fig.7. Validating process of 3rd order HONU at current density of 4.00 A·dm⁻²

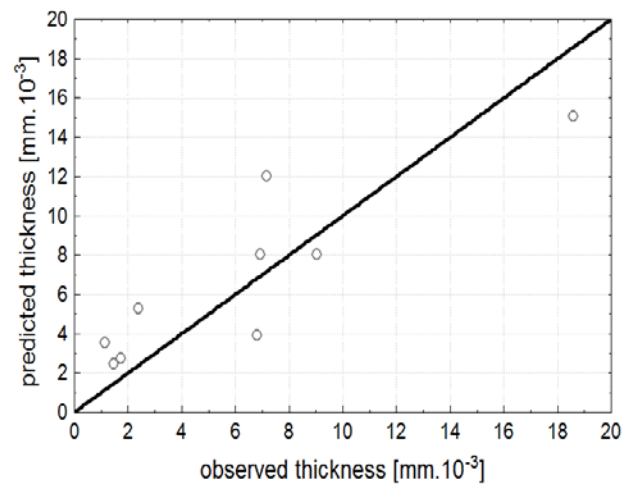


Fig. 8. Validating process of 3rd order HONU at current density of 5.00 A·dm⁻²

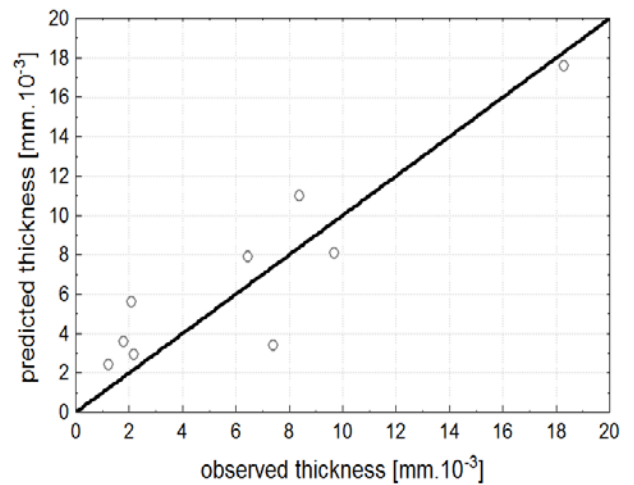


Fig. 9. Validating process of 3rd order HONU at current density of 6.00 A·dm⁻²

Tab. 3 shows the chosen statistical stats of correctness of used models through the validation process for the current densities of 4.00, 5.00 and 6.00 A·dm⁻². As is shown, the sum of square errors within model validation process for cubic neural unit reaches the values of 87.51 mm²·10⁻⁶, 62.42 mm²·10⁻⁶ and 45.31 mm²·10⁻⁶ according to the individual current densities. The sums of squared errors when using the cubic neural units are generally ten times less than the sum of squared errors when using linear or quadratic neural units. Mean squared errors (MSE) of estimations are 1.90 mm·10⁻⁶, 1.36 mm·10⁻⁶ and 0.98 mm·10⁻⁶ for individual current densities 4.00, 5.00 and 6.00 A·dm⁻² and those errors are also ten times less than MSE when using the linear neural unit or quadratic neural unit. The confidence interval of cubic neural unit is 70.23 %, 72.57 % and 82.05 % according to the individual current densities of 4.00, 5.00 and 6.00 A·dm⁻². These values also mean the accuracy of estimation of formed AAO layer thickness based on various combinations of the input factors.

Table 3. Selected indicators of the accuracy of developed models

Model	Current density [A·dm ⁻²]	SSE [-]	MSE [-]	R ² [%]	R [%]
Cubic 3 rd Order HONU	4.00	87.51	1.90	0.89	0.94
	5.00	62.42	1.36	0.86	0.93
	6.00	45.31	0.98	0.87	0.93
Quadratic 2 nd Order HONU	4.00	656.75	14.28	0.82	0.90
	5.00	519.70	11.30	0.80	0.90
	6.00	335.50	7.29	0.82	0.90
Linear 1 st Order HONU	4.00	518.69	11.28	0.64	0.80
	5.00	649.87	14.13	0.64	0.80
	6.00	496.92	10.80	0.64	0.80

Using the developed computational models it is also possible to monitor the influence of individual input factors on the final thickness of AAO layer. To illustrate it, the graphical interpretation of dependencies, describing the effect of individual factors on the final thickness of AAO layer at current densities of 4:00, 5:00 and 6:00 Adm⁻², was created. The level of only one factor was varied; the level of the remaining five factors was set at level 0. Fig. 10 – Fig. 15 display the effect of these factors.

The effect of factor x_1 is displayed in Fig. 10, the effect of factor x_2 in Fig. 11, the effect of factor x_3 in Fig. 12, the effect of factor x_4 in Fig. 13, the effect of factor x_5 in Fig. 14 and the effect of factor x_6 in Fig. 15. As seen in Fig. 10 – Fig. 15, the size of the current density has no noticeable effect on the thickness of the AAO layer in those areas where formation of the layer occurs. Respectively, the effect of current density is minimal (for boundary conditions, the difference in thickness of the AAO layer is less than $2\text{mm}\cdot 10^{-3}$).

Fig. 10 shows influence of factor x_1 on AAO layer thickness. Factor x_2 , x_3 , x_4 , x_5 and x_6 are set to zero factor level. We can see that with increasing of amount of sulphuric acid is also increasing AAO layer thickness. It is because with an increasing amount of sulphuric acid in an electrolyte also rises an amount of dissociated ions. Oxygen, which is bound to a part of these ions, is used to create a layer of an aluminium oxide. Thus, more dissociated oxygen ions means coarser AAO layer thickness.

Fig. 11 shows influence of factor x_2 on AAO layer thickness. Factor x_1 , x_3 , x_4 , x_5 and x_6 are set to zero factor level. We can see that with increasing of amount of oxalic acid is also increasing AAO layer thickness until it is reach zero factor level. After that the created AAO layer thickness starts decreasing. It is because the molecules of oxalic acid need a bigger inner energy to dissociate. Applied voltage is not big enough to raise their inner energy. So the molecules of oxalic acid take the energy from an electrolyte including from sulphuric acid molecules. Thus, the molecules of sulphuric

acid cannot dissociate and amount of oxygen in electrolyte is decreasing. Fortunately the amount of oxalic acid is not very big so the maximum possible difference of layer thickness is just up to $5\text{mm}\cdot 10^{-3}$.

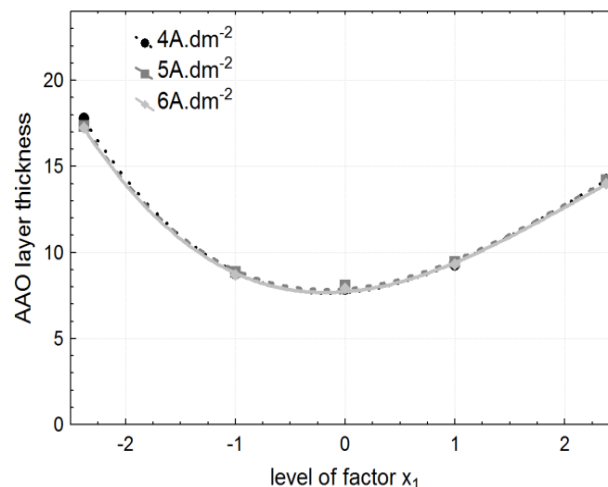


Fig. 10 Effect of factor x_1 on the thickness of AAO layer at given conditions $x_2=0$ ($1.22\cdot 10^{-1}\text{ mol}\cdot\text{l}^{-1}$), $x_3=0$ ($3.15\cdot 10^{-1}\text{ mol}\cdot\text{l}^{-1}$), $x_4=0$ ($22.00\text{ }^\circ\text{C}$), $x_5=0$ (1800.00 s), $x_6=0$ (10.00 V)

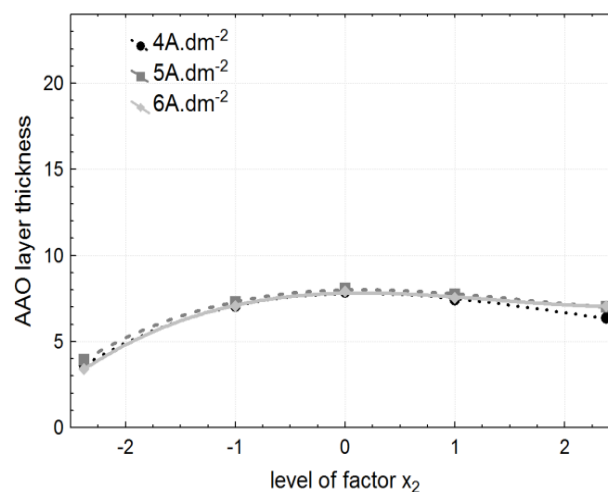


Fig. 11 Effect of factor x_2 on the thickness of AAO layer at given conditions $x_1=0$ ($2.04\cdot 10^{-1}\text{ mol}\cdot\text{l}^{-1}$), $x_3=0$ ($3.15\cdot 10^{-1}\text{ mol}\cdot\text{l}^{-1}$), $x_4=0$ ($22.00\text{ }^\circ\text{C}$), $x_5=0$ (1800.00 s), $x_6=0$ (10.00 V)

In Fig. 12 it is presented the influence of factor x_3 on the thickness of the formed aluminium anodic oxide layer. Factors x_1 , x_2 , x_4 , x_5 and x_6 are set to zero factor level. From the Fig. 12 it can be deduced that low levels of factor x_3 lead to the dissolution of the oxide layer and to the saturation of the electrolyte of aluminum cations Al^{3+} . If the concentration of the aluminum cations in the electrolyte is higher than at the steady state, it results in their migration to the cathode where they are reduced to atomic aluminum and the system energy is decreased. It is similar to the impact of the concentration of oxalic acid in electrolyte on the resulting thickness of the formed anodic aluminum oxide layer.

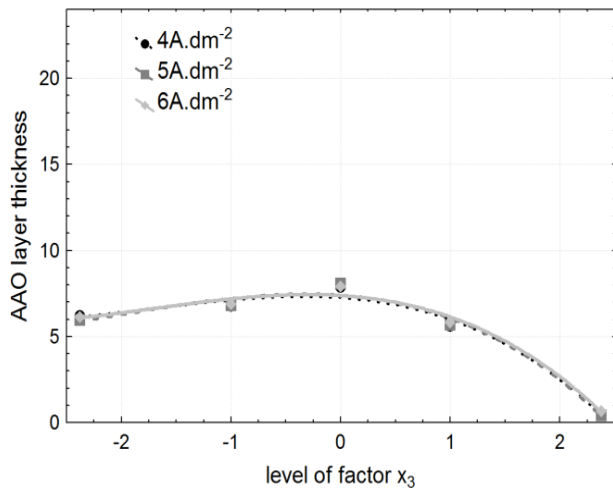


Fig. 12 Effect of factor x_3 on the thickness of AAO layer at given conditions $x_1=0$ ($2.04 \cdot 10^{-1} \text{ mol}\cdot\text{l}^{-1}$), $x_2=0$ ($1.22 \cdot 10^{-1} \text{ mol}\cdot\text{l}^{-1}$), $x_4=0$ ($22.00 \text{ }^\circ\text{C}$), $x_5=0$ (1800.00 s), $x_6=0$ (10.00 V)

Fig. 13 shows influence of factor x_4 on AAO layer thickness. Factor x_1, x_2, x_3, x_5 and x_6 are set to zero factor level. The electrolyte temperature influences the speed of chemical reactions at the interface metal-electrolyte. Those reactions are creating AAO layer thickness and dissolving already created AAO layer thickness. The speed of chemical reactions which creating and dissolving the AAO layer is different during anodizing, but generally with increasing of electrolyte temperature is speed of chemical reactions increasing too. It means that with increasing of electrolyte temperature will be AAO layer thickness coarser.

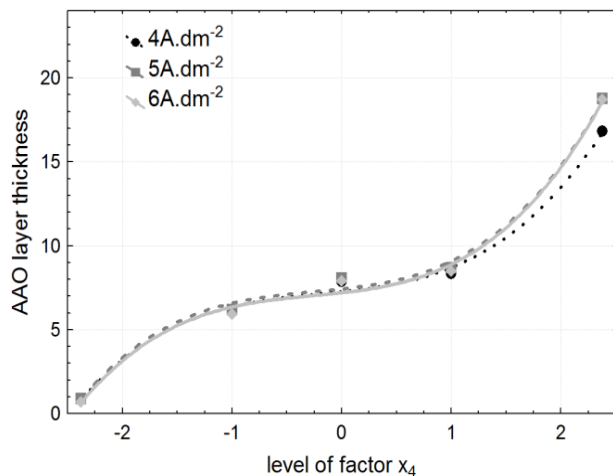


Fig. 13 Effect of factor x_4 on the thickness of AAO layer at given conditions $x_1=0$ ($2.04 \cdot 10^{-1} \text{ mol}\cdot\text{l}^{-1}$), $x_2=0$ ($1.22 \cdot 10^{-1} \text{ mol}\cdot\text{l}^{-1}$), $x_3=0$ ($3.15 \cdot 10^{-1} \text{ mol}\cdot\text{l}^{-1}$), $x_5=0$ (1800.00 s), $x_6=0$ (10.00 V)

Fig. 14 shows influence of factor x_5 on AAO layer thickness. Factor x_1, x_2, x_3, x_4 and x_6 are set to zero factor level. The anodizing time influences how long are chemical reactions go on. With increasing of anodizing time is AAO layer thickness rising. But speed of AAO layer thickness rising depend on speed of chemicals reactions at metal-electrolyte interface.

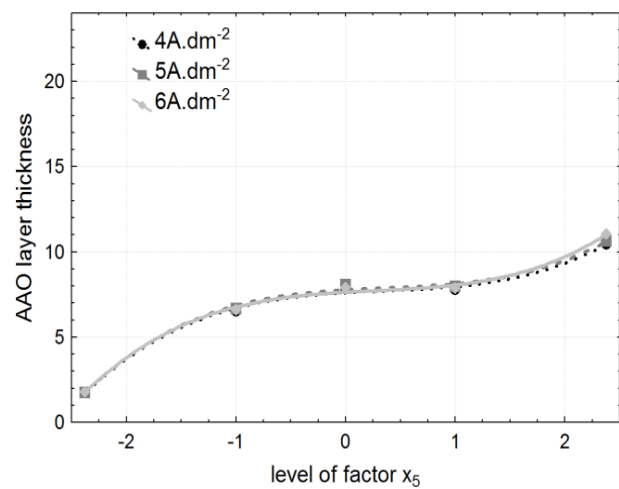


Fig. 14 Effect of factor x_5 on the thickness of AAO layer at given conditions $x_1=0$ ($2.04 \cdot 10^{-1} \text{ mol}\cdot\text{l}^{-1}$), $x_2=0$ ($1.22 \cdot 10^{-1} \text{ mol}\cdot\text{l}^{-1}$), $x_3=0$ ($3.15 \cdot 10^{-1} \text{ mol}\cdot\text{l}^{-1}$), $x_4=0$ ($22.00 \text{ }^\circ\text{C}$), $x_6=0$ (10.00 V)

Finally Fig. 15 shows influence of factor x_6 on AAO layer thickness. Factor x_1, x_2, x_3, x_4 and x_5 are set to zero factor level. Applied voltage levels are proportional to the electric potential. Electric potential is proportional to electrodynamic forces. These electrodynamic forces determine the force with which are positively charged ions attracted to the negatively charged electrode (cathode) and the force with which are negatively charged ions attracted to the positively charged electrode (anode). So with increasing of applied voltage also increase an AAO layer thickness.

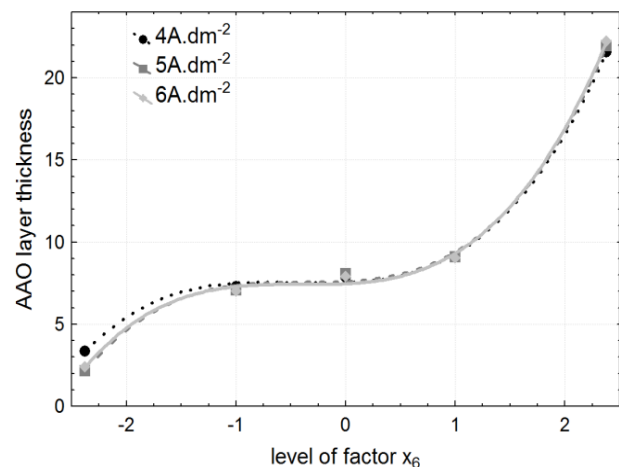


Fig. 15 Effect of factor x_6 on the thickness of AAO layer at given conditions $x_1=0$ ($2.04 \cdot 10^{-1} \text{ mol}\cdot\text{l}^{-1}$), $x_2=0$ ($1.22 \cdot 10^{-1} \text{ mol}\cdot\text{l}^{-1}$), $x_3=0$ ($3.15 \cdot 10^{-1} \text{ mol}\cdot\text{l}^{-1}$), $x_4=0$ ($22.00 \text{ }^\circ\text{C}$), $x_5=0$ (1800.00 s)

IV. CONCLUSION

As shown by the evaluation of experimental results presented above, the use of neural networks based on the iterative Levenberg-Marquardt (LM) optimization algorithm provides a wide range of options to control the anodizing process. There are several reasons for this. First and foremost, there is a pressing need to produce the right product at the

right time, and here the use of neural networks comes in very handy. We can quickly and simply describe the behavior of the monitored system. By using the neural unit of 3rd order HONU it was possible to describe the influence of input factors on the thickness of final AAO layer at defined current densities 4.00 A·dm⁻², 5.00 A·dm⁻² and 6.00 A·dm⁻² with confidence interval of 93.45%, 95.17% and 96.69%. This neural unit allowed us to monitor the impact of input factors on the final thickness of the AAO layer. It also provide us another way of understanding and expressing the process behavior by graphical representation of how a response (the thickness of AAO layer) may change due to changing values of factors $x_1 - x_6$ and their interactions.

ACKNOWLEDGMENT

The research work is supported by the Project of the Structural Funds of the EU, Operational Programme Research and Development, Measure 2.2 Transfer of knowledge and technology from research and development into practice. Title of the project: „Research and development of intelligent nonconventional actuators based on artificial muscles”, ITMS code: 26220220103 and IÚ 1/2013 Modelling of surface treatment processes of selected materials.

REFERENCES

- [1] J. Baumeister, J. Banhart, M. Weber, “Aluminium foams for transport industry,” *Materials & Design*, vol. 18, no. 4, 1997, pp. 217-220
- [2] F. King, “Aluminium and its alloys,” UK: Ellis Horwood Limited, 1987
- [3] L. A. Dobrzański, M. Krupinski, J. H. Sokolowski, “Computer aided classification of flaws occurred during casting of aluminum,” *Journal of Materials Processing Technology* 167, 2005, pp. 456-462
- [4] W. Mingliang, L. Yinong, Y. Hong, “A unified thermodynamic theory for the formation of anodized metal oxide,” *Structures Electrochimica Acta*, vol. 62, 2012, pp. 424-432
- [5] G. K. Singh, A. A. Golovin, I. S. Aranson, V. M. Vinokur, “Formation of nanoscale pore arrays during anodization of aluminum,” *Europhysics Letters*, vol. 70(6), 2005, pp. 836-842
- [6] Z. Meng, S. I. Masatoshi, J. Himendra, “Influence of desiccation procedures on the surface wettability and corrosion resistance of porous aluminium anodic oxide films,” *Sorrosion Science*, vol. 55, 2012, pp. 332-338
- [7] M. Gombár, A. Vagaská, J. Kmec, P. Michal, “Microhardness of the coatings created by anodic oxidation of aluminium,” *Applied Mechanics and Materials*, vol. 308, 2013, pp. 95-100 ISSN 1660-9336
- [8] A. Vagaská, M. Gombár, J. Kmec, P. Michal, “Statistical analysis of the factors effect on the zinc coating thickness,” *Applied Mechanics and Materials*, vol. 378, 2013, pp. 184-189
- [9] P. Michal, M. Gombár, A. Vagaská, J. Piteľ, J. Kmec, “Experimental study and modeling of the zinc coating thickness,” *Advanced Materials Research*, vol. 712-715, 2013, pp. 382-386
- [10] A. Panda, J. Jurko, M. Džupon, I. Pandová, “Optimalization of heat treatment bearings rings with goal to eliminate deformation of material,” *Chemické listy (Chemical Letters)*, vol. 105, no. S. (2011)
- [11] M. Badida, M. Gombár, L. Sobotová, J. Kmec, “Determination of electroless deposition by chemical nickeling,” In: *Environmental and Light Industry Technologies, 3rd Int. Joint Conference*, 2012, Budapest, Hungary – Budapest: Óbuda University, 2012, p. 27-38,
- [12] E. Straka, I. Čorný, J. Boržiková, “Analysis of heat – affected zone depth of sample surface at electrical discharge machining with brass wire electrode,” *Strojstvo: Journal for Theory and Application in Mechanical Engineering*, vo. 51, 2009, No. 6, pp. 633-640
- [13] M. Gombár, L. Sobotová, M. Badida, J. Kmec, “The comparison of possibilities at using of different electrolytes in the process of anodizing aluminium,” *Metallurgija*, vol. 53, No. 1, 2014, p. 47-50 ISSN 0543-5846
- [14] N. Kobasko, “Intense Hardening of Optimal Hardenability Steels Saves Alloy Elements, Energy, Improves Service Life of Machine Components and Makes Environment Cleaner,” In: *Advances in Modern Mechanical Engineering, FLUIDSHEAT '13, Croatia 2013*, published by WSEAS Press, ISSN: 2227-4596
- [15] J. Mižáková, J. Piteľ, “The numerical approximation of function of transient response,” In: *Matematické metody v technike I technologijach. Tom 7. – Jaroslavl: Jaroslavskij gosudarstvennyj techničeskij univesitet*, 2007, pp. 243-244, ISBN 5230207094
- [16] J. Mižáková, “The support of the applied mathematics by chosen programming languages,” In: *7. Mathematical workshop, Brno: VUT*, 2008, pp. 1-4, ISBN 9788021437272
- [17] S. Hrehová, A. Vagaská, “Application of fuzzy principles in evaluating quality of manufacturing process,” *WSEAS Transaction on Power Systems*, vol. 7, No. 2, 2012, pp. 50-59, ISSN 1790-5060
- [18] A. Macurová, S. Hrehová, “Some properties of the pneumatic artificial muscle expressed by the nonlinear differential equation,” *Advanced Materials Research*, vol. 658, 2013, Trans Tech Publications Switzerland, p. 376-379, ISSN 1022-6680
- [19] S. Hrehová, “Solution of differential equation using a support of some software programs,” In: *Chapters about Solutions Differential Equations Systems and Some Applications Differential Equations*, Brno: Tribun eU, 2009, pp. 59-70, [1.45]
- [20] Durmus Karazel, “Prediction and control of surface roughness in CNC lathe using artificial neural network,” *Journal of Materials Processing Technology*, vol. 209, 2009, pp. 3125-3137
- [21] L. E. Zárate, F. R. Bittencout, “Representation and control of the cold rolling process through artificial neural networks via sensitivity factors,” *Journal of Materials Processing Technology* 197, 2008, pp. 344-362
- [22] A. M. Hassan, A. Alrashdan, M. T. Hayajneh, A. T. Mayyas, “Prediction of density, porosity and hardness in aluminum-copper-based composite materials using artificial neural network,” *Journal of Materials Processing Technology*, vol. 209, 2009, pp. 894-899
- [23] J. Piteľ, J. Mižák, “Computational intelligence and low cost sensors in biomass combustion process, Proceedings of the 2013 IEEE (SSCI), Symposium Series on Computational Intelligence in Control and Automation (CICA), Singapore: IEEE, 2013, pp. 165-168
- [24] A. Hošovský, K. Židek, C. Oswald, “Hybridized GA-optimization of neural dynamic model for nonlinear process, Proceedings of the 2012 13th Intern. Carpathian Control Conference (ICCC), Košice: IEEE, 2012, pp. 227-232
- [25] M. Gupta, i. Bukovsky, N. Homma, M. G. A. Solo, Z. G. Hou, “Fundamentals of higher order neural networks for modeling and simulation,” *Artificial Higher Order Neural Networks for Modelin and Simulation*, ed. M. Zhang, IGI Global, 2012
- [26] I. Bukovsky, M. Lepold, J. Bila, “Quadratic neural unit and its network in validation of process data of steam turbine loop and energetic boiler,” *WCCI 2010, IEEE Int. Joint. Conf. on Neural Networks, IJCNN*, Barcelona, Spain, 2010
- [27] R. Rodriguez, I. Bukovsky, N. Homma, “Potentials of quadratic neural unit for applications,” *Int. Journal of Software Science and Computational Intelligence (IJSSCI)*, vol. 3, issue 3, IGI Global, Publishing, Hershey PA, USA, 2011, pp. 1-12, ISSN 1942-9045
- [28] I. Bukovsky, N. Homma, L. Smetana, R. Rodriguez, M. Mironovova, S. Vrana, “quadratic neural unit is a good compromise between linear models and neural networks for industrial applications, ICCI 2010, The 9th IEEE Inter. Conference on Cognitive Informatics, Tsinghua University, Beijing, China, July 7-9, 2010